Thin Solid Films 664 (2018) 19–26

Contents lists available at ScienceDirect

Thin Solid Films

journal homepage: www.elsevier.com/locate/tsf

Growth and characterization of ZnS_xSe_{1-x} thin films deposited by spray pyrolysis

Nandkishor M. Patil, Santosh G. Nilange, Abhijit A. Yadav*

Thin Film Physics Laboratory, Department of Physics, Electronics and Photonics, Rajarshi Shahu Mahavidyalaya, Latur 413512, Maharashtra, India

ARTICLE INFO

Keywords:
Thin films
Spray pyrolysis
Growth mechanism
X-ray diffraction
Semiconducting materials
Optical properties
Electrical properties

ABSTRACT

In this work, zinc sulphoselenide ZnS_xSe_{1-x}; ($0.0 \le x \le 1.0$) thin films were grown on glass substrates using a computerized chemical spray pyrolysis. The mechanism of growth and the structural, morphological, compositional, optical and electrical properties were studied. An X-ray diffraction study confirmed that the polycrystalline ZnS_xSe_{1-x} thin films had a cubic zinc blende structure with a preferential ⟨111⟩ orientation. The shift in the peak < 111 > direction towards higher 2θ values with increasing sulfur concentration confirmed the formation of a solid solution. The crystallite size was observed to be in the range 18–28 nm. Using energy dispersive X-ray spectroscopy, the formation of nearly stoichiometric ZnS_xSe_{1-x} thin films was confirmed. The optical band gap increased from 2.84 eV to 3.57 eV when the composition of the ZnS_xSe_{1-x} was changed. The thin films were found to be semiconducting in nature. The observed tunable optical and electrical properties of the ZnS_xSe_{1-x} thin films suggest that they can be used for a wide range of optoelectronic applications.

1. Introduction

During the last few decades, different properties of binary and ternary II–VI semiconductor materials have been studied and applications in various devices have been developed [1–5]. These applications include nuclear, industrial and medicinal applications [6]. II-VI semiconductor materials are extensively used in quantum wells, quantum dots, quantum wires, optoelectronic devices, lasing devices, and detectors in nuclear power plants and solar cells [7,8].

There are many II–VI group semiconducting materials, including cadmium selenide (CdSe), cadmium sulfide (CdS) [2,4,9] cadmium telluride (CdTe) [10], zinc oxide (ZnO), zinc selenide (ZnSe), zinc sulfide (ZnS) and zinc telluride (ZnTe) [11]. ZnS and ZnSe have proved to be useful for fabricating a wide range of optoelectronic devices due to their low toxicity, low cost, low resistivity, wide band gap, non-pollutant nature, high photosensitivity and abundance in the Earth's crust [12–17]. However, for some optoelectronic applications, it is necessary to tune the band gap, and this can be achieved through composition modulation. In ternary compounds, the band gap can be tuned by simply adjusting the composition [18]. ZnSSe alloys potentially have many applications since the band gap can be tuned by changing the proportions of the constituent elements.

There are various methods of preparing II–VI compounds, including sputtering [19], molecular beam epitaxy [20], vacuum evaporation [21], atomic layer epitaxy [22], hydrogen vapor transport [23], solvothermal synthesis [24], sintering [25], close–spaced sublimation [26], chemical bath deposition [27], and spray pyrolysis [28–30]. Spray pyrolysis is a simple, low cost method. It yields high quality films that are suitable for use in devices such as solar cells. Unlike other methods, spray pyrolysis does not require high quality substrates or chemicals. The rate of deposition can be controlled easily, and there is little loss of material. It has been reported in the literature that spray deposited films are highly uniform, pinhole-free, strong and stable with time and temperature [14]. In the present work, zinc sulphoselenide (ZnS_xSe_{1-x};$0.0 \le x \le 1.0$) thin films were deposited by chemical spray pyrolysis on glass substrates at deposition temperatures of 275 °C. The growth mechanism and the structural, morphological, compositional, optical and electrical properties of these thin films were studied.

2. Experimental

2.1. Deposition of thin films

ZnS_xSe_{1-x} ($0.0 \le x \le 1.0$) thin films were deposited using a computerized chemical spray pyrolysis setup shown in Fig. 1. Soda-lime glass microslides of size 7.5 cm × 2.5 cm and thickness 0.135 cm (Blue Star Corporation, Mumbai), were used as substrates. The substrates were cleaned using the procedure described in Reference [31]. When

* Corresponding author.
E-mail address: aay_physics@yahoo.co.in (A.A. Yadav).

https://doi.org/10.1016/j.tsf.2018.08.018
Received 8 October 2017; Received in revised form 14 August 2018; Accepted 14 August 2018
Available online 20 August 2018

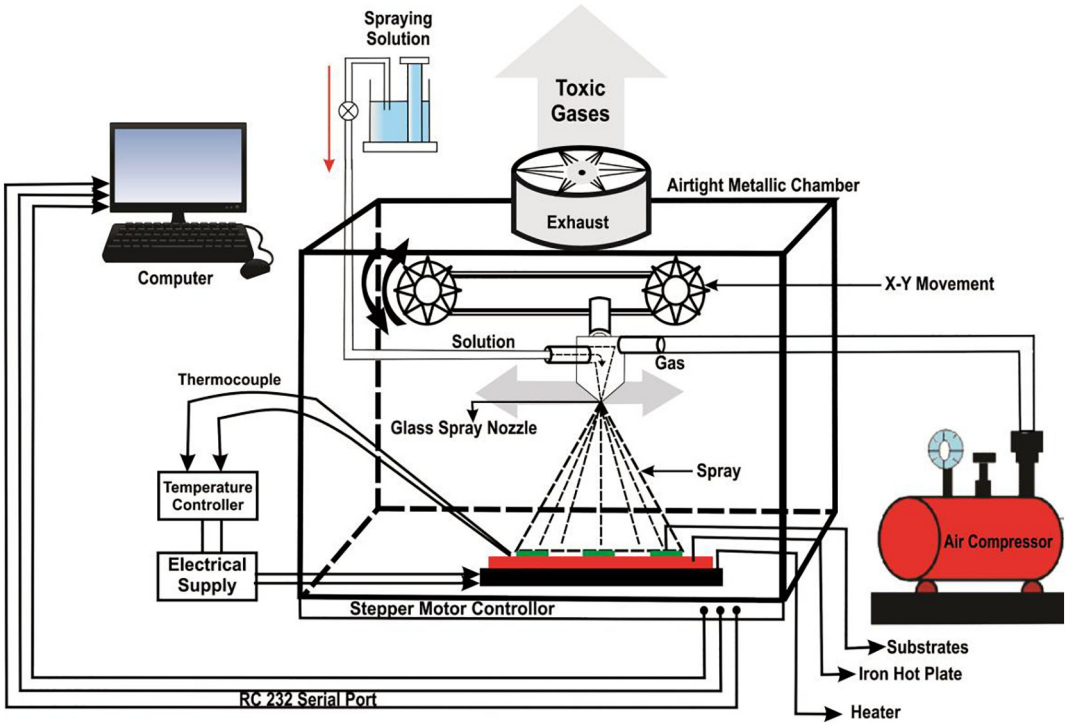

Fig. 1. Schematic illustration of the computerized chemical spray pyrolysis set up used for ZnS_xSe_{1-x} thin film deposition.

the preparative parameters were being optimized, fluorine-doped tin oxide (FTO)-coated glass substrates were used. Details of the procedures used for deposition on the FTO-coated glass substrates are given in Reference [32].

2.1.1. Deposition of ZnS thin film

Equimolar solutions containing precursors of zinc chloride (purity 99.5%) and thiourea (purity 99.5%) were prepared by dissolving suitable amounts of these salts (A.R. grade) in double distilled water. These equimolar solutions were then mixed together in appropriate volumes to obtain the Zn:S ratio of 1:1 (stock solution). The final spraying solution was prepared by mixing 20 cc of this stock solution with 20 cc of isopropyl alcohol (purity 99.7%). This solution was sprayed through an air–blast atomizer glass nozzle (diameter 0.048 cm) onto preheated glass and FTO–coated glass (sheet resistance of 8–10 Ω/cm^2) substrates. The atomization of the aqueous solution into a spray of fine droplets was effected using an automatic (computer controlled) air-blast atomizer type glass nozzle, with compressed air serving as the carrier gas.

Optimization of preparative parameters of photoactive semiconducting electrodes by photoelectrochemical (PEC) method is a reliable and unique technique used in thin film research. The PEC technique involves testing the photosensitivity of an electrode for optimum values of the short circuit current (Isc) and open circuit voltage (Voc) in a PEC cell formed with a semiconducting electrode along with the counter electrode in an appropriate redox electrolyte (in the present case 1 M polysulfide) [33]. The deposition temperature and solution concentration were optimized using the PEC technique.

The experiments were carried out in two sets: in the first set, the deposition temperature (temperature of hot plate) was varied from 225 °C, at intervals of 25 °C, to 325 °C all other parameters constant, especially the concentration of the spraying solution (0.025 M). The hot plate temperature (deposition temperature) was controlled using an iron-constantan thermocouple. In this process, the substrates were heated by using an electrical heater with heating coil (2000 W). The films deposited on FTO-coated glass substrates were used in PEC cells. Films deposited at 275 °C displayed the highest photosensitivity, and so the optimized deposition temperature was 275 °C. In second set, the deposition temperature was kept fixed at 275 °C and spraying solutions of concentration 0.025 M, 0.0375 M, 0.050 M and 0.0625 M were used. The films were used in PEC cells. It was noted that the films deposited with the spraying solution of concentration 0.05 M displayed the highest photosensitivity, and so the optimized concentration was 0.05 M. In a similar fashion the other parameters were optimized: spray rate, 3 $ccmin^{-1}$; deposition time, 13–14 min; carrier gas pressure 176,520 N m^{-2}; the distance between the substrate and the nozzle (head of spray source), 30 cm.

2.1.2. Deposition of ZnSe thin film

A similar procedure was used to deposit ZnSe thin films, with selenourea (purity 99.9 + %) used instead of thiourea.

2.1.3. Deposition of ZnS_xSe_{1-x} ($0.0 \le x \le 1.0$)

From the PEC studies carried out on ZnS and ZnSe thin films, it was seen that the optimized conditions were the same for both types of thin films. Therefore all the deposition conditions were maintained constant at the optimized values (deposition temperature, 275 °C; solution concentration 0.05 M; spray rate, 3 $ccmin^{-1}$; deposition time, 13–14 min; air as the carrier gas, at a pressure of 176,520 N m^{-2}; the distance between the substrate and the nozzle, 30 cm). However, the stock solution was prepared by mixing zinc chloride, thiourea and selenourea together in an appropriate proportion to obtain a Zn:(S + Se) ratio of 1:1. The final spraying solution was prepared by mixing 20 cc of the stock solution with 20 cc of isopropyl alcohol. In a different set of experiments, the values of composition parameter (x) were adjusted by varying the proportions of thiourea (S) and selenourea (Se). After deposition, the films were allowed to cool at room temperature. The adhesion of the films on the substrate as measured using a tape test was fairly good.

2.2. Characterization of ZnS_xSe_{1-x} ($0.0 \le x \le 1.0$) thin films

The ZnS_xSe_{1-x} thin films were characterized in terms of their structural, morphological, compositional, optical and electrical

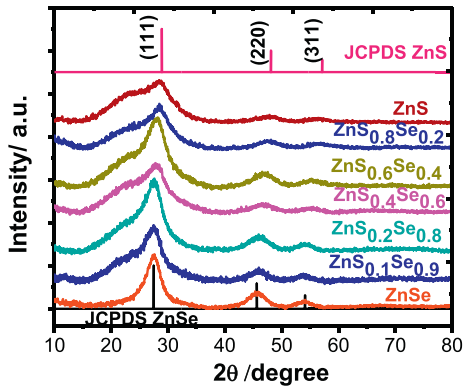

Fig. 2. XRD patterns of spray deposited ZnS_xSe_{1-x} thin films.

properties. The thickness of the as deposited films was measured by a well–known gravimetric weight difference method. A sensitive microbalance was used, and the bulk density of the ZnS_xSe_{1-x} was assumed. Structural analysis of the thin films was performed using a Philips PW-3710 X-ray diffractometer with Cu-K_α radiation, within the 2θ range from 10 to 80°. The surface morphology was analyzed and compositional analysis of the thin films spray deposited on glass substrates was carried out using an FEI Quanta 200 scanning electron microscope (SEM) and Octane plus EDX energy-dispersive X-ray spectroscopy (EDS) system. EDS analysis was used to determine the atomic percentage of zinc (Zn), sulfur (S) and selenium (Se) present in the thin films. A UV–Visible spectrophotometer (JAZ Spectrometer, Ocean optics) was used to record the optical absorption spectra. Electrical resistivity measurements were carried out using the DC two point probe technique. Silver paste was painted in a "two bar" pattern (thickness of painted silver,1 mm; length of bar, 1 cm; distance between two bars, 1 cm) on the ZnS_xSe_{1-x} thin films to ensure that good ohmic contacts were established.

3. Results and discussion

3.1. Growth mechanism

In spray pyrolysis, the precursor solution is pulverized using an air so that it reaches the hot substrate in the form of very fine droplets. The constituents react to form a chemical compound onto the hot substrate. Physical inspection of as deposited films shows that the light-yellow colour of ZnSe changes to the whitish colour of ZnS as the composition parameter (x) changes from 0 to 1. This change in colour with 'x' indicates the substitution of Se^{2-} ions by S^{2-} ions in the ZnSe lattice. The terminal thicknesses of the thin films, measured using the gravimetric weight difference method, were found to be 260 nm for ZnSe, 271 nm for x = 0.1, 275 nm for x = 0.2, 280 nm for x = 0.4, 270 nm for x = 0.6, 255 nm for x = 0.8, and 243 nm for ZnS. The thickness was confirmed from cross-sectional SEM images of the $ZnS_{0.2}Se_{0.8}$ thin films. The values obtained using the gravimetric weight difference method and cross-sectional scanning electron microscopy were found to be nearly the same. Therefore the thickness values obtained using the gravimetric weight difference method were used for further calculations.

Leigh et al. [23] have discussed the reaction mechanism of ZnS_xSe_{1-x} thin films heteroepitaxially deposited by hydrogen vapor transport in an open-tube reactor. The relevant equations governing the deposition of ZnS_xSe_{1-x} thin films are specified. The vapor pressures of Se and S are neglected since their contributions to the total pressure are negligible. It was concluded that the composition of the alloy phase corresponds to the partial pressures of the reactants (H_2S and H_2Se) in the vapor phase. Taking an idea from Leigh's work, a simple reaction mechanism for the growth of ZnS_xSe_{1-x} films was proposed:

The selenide ions are released by the decomposition of selenourea according to the following equations,

$$\begin{array}{l} NH_2 \\ | \\ NH_2 - C = Se \end{array} + OH^- \rightarrow CH_2N_2 + H_2O + HSe^- \quad (1)$$

$$HSe^- + OH^- \rightarrow Se^{2-} + H_2O \quad (2)$$

Similarly sulfate ions are released by decomposition of thiourea according to the following equations,

$$\begin{array}{l} NH_2 \\ | \\ NH_2 - C = S \end{array} + OH^- \rightarrow CH_2N_2 + H_2O + HS^- \quad (3)$$

$$HS^- + OH^- \rightarrow S^{2-} + H_2O \quad (4)$$

In the presence of metal zinc ions the chemical reaction will be,

$$Zn^{2+} + xS^{2-} + (1 - x)\,Se^{2-} \rightarrow ZnS_xSe_{1-x} + \text{volatile products} \quad (5)$$

3.2. Structural studies

The ZnS_xSe_{1-x} thin films deposited at 275 °C were characterized using XRD. Generally ZnS and ZnSe exist in two main crystalline forms, wurtzite (hexagonal) and zinc blende (cubic). Fig. 2 displays a typical XRD pattern of the spray-deposited thin films. Each diffraction pattern relates to different values of x (x = 0, 0.1, 0.2, 0.4, 0.6, 0.8 and 1.0) in the precursor solution of the ZnS_xSe_{1-x}. It may be observed that the films are polycrystalline over the entire composition range. From Fig. 2, it may be seen that the characteristic peaks of ZnS_xSe_{1-x} (x = 1.0; ZnS) are along the < 111 > , ⟨220⟩ and ⟨311⟩ directions and are located at 28.15°, 47.70° and 56.50°, respectively, with preferential orientation along the < 111 > direction. The matching of the observed and standard 'd' values confirmed that the ZnS thin film is in the cubic phase (JCPDS data card 80–0022). Formation of the cubic phase of ZnS using spray pyrolysis with aqueous solutions of thiourea and zinc acetate was reported by Diabat et al. [34]. For x = 0 (ZnSe), the principal orientation is along at 27.29°, with peaks of < 220 > and < 311 > at 45.32° and 53.07°, respectively. Comparison of the observed data with the standard JCPDS (card 80–0021) showed that the ZnSe thin films had a cubic (zinc blende) structure. Analogous results were obtained by Yadav et al. [35] for ZnSe synthesized via a simple hydrothermal route. For the intermediate compositions (x = 0.1, 0.2, 0.4, 0.6, 0.8), with increasing 'x' there is a shifting of the peak position towards higher 2θ values, suggesting the formation of solid solutions. Similar results were obtained by Subbaiah and coworkers [14] for ZnS_xSe_{1-x} films deposited using close-spaced evaporation.

The lattice parameter (a) is calculated using the standard relation for the cubic phase,

$$\frac{1}{d^2} = \frac{h^2 + k^2 + l^2}{a^2} \quad (6)$$

where h, k, and l are the Miller indices and d is the interplanar spacing calculated using Bragg's relation ($n\lambda = 2d\sin\theta$). Table 1 shows the lattice constants and interplanar spacing values calculated from the XRD results. Fig. 3 shows the variation of the lattice parameter with the composition (x) of the ZnS_xSe_{1-x} thin films. The plot of 'a' versus 'x' is almost a straight line and shows an appropriate mixing of ZnS and ZnSe to form ZnS_xSe_{1-x} thin films. As the sulfur content of the films increases the lattice constants of the ZnS_xSe_{1-x} thin films decreases linearly according to the relation,

$$a = 5.648\,(1 - x) + 5.368x \quad (7)$$

This behavior of the lattice parameter is in accordance with Vegard's

Table 1
Various structural parameters of spray deposited ZnS_xSe_{1-x} ($0.0 \le x \le 1.0$) thin films.

Composition	2θ	d (Å)		hkl	a	Crystallite Size
	(°)	Observed	Standard		(Å)	D (nm)
ZnSe	27.29	3.265	3.244	111	5.648	22
	45.32	1.999	1.986	220		
	53.07	1.724	1.694	311		
$ZnS_{0.1}Se_{0.9}$	27.34	3.259	3.227	111	5.612	24
	45.44	1.994	1.976	220		
	53.32	1.717	1.686	311		
$ZnS_{0.2}Se_{0.8}$	27.42	3.25	3.212	111	5.586	28
	45.74	1.982	1.967	220		
	53.57	1.709	1.677	311		
$ZnS_{0.4}Se_{0.6}$	27.76	3.211	3.18	111	5.532	26
	46.07	1.968	1.948	220		
	54.85	1.672	1.661	311		
$ZnS_{0.6}Se_{0.4}$	28.02	3.181	3.149	111	5.478	23
	46.91	1.935	1.928	220		
	55.15	1.664	1.644	311		
$ZnS_{0.8}Se_{0.2}$	28.45	3.134	3.117	111	5.419	21
	47.33	1.919	1.909	220		
	55.89	1.644	1.628	311		
ZnS	28.15	3.167	3.086	111	5.368	18
	47.7	1.905	1.89	220		
	56.5	1.627	1.611	311		

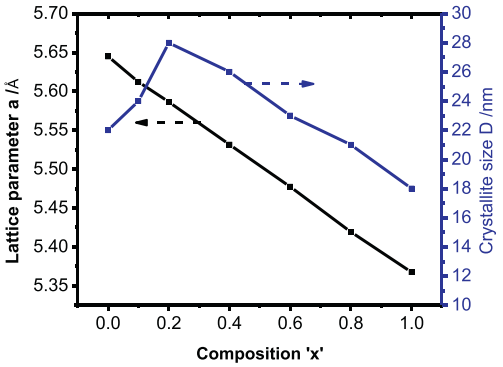

Fig. 3. Variation of lattice parameter 'a' and crystallite size 'D' with composition '*x*' for spray deposited ZnS_xSe_{1-x} thin films.

law [8], confirming the formation of a solid solution in the ZnS_xSe_{1-x} thin films.

The crystallite size (D), of the ZnS_xSe_{1-x} was estimated using Debye-Scherrer's formula [36],

$$D = \frac{k\lambda}{\beta\cos\theta} \tag{8}$$

where λ is the wavelength of X-ray used (1.54056 Å), β is the full width at half of the peak maximum measured in radians, θ is Bragg's angle and k = 0.9. While measuring the crystallite size, the value of β is corrected by subtracting the instrumental factor b. The crystallite sizes are estimated for the standard < 111 > direction and are summarized in Table 1. They fall within the range 18–28 nm. Fig. 3 shows the variation of crystallite size with composition, 'x'. It should be noted that the crystallite size increases with increasing 'x' in the ZnS_xSe_{1-x} thin films, reaches a maximum of 28 nm at x = 0.2 and decreases thereafter with a further increase in 'x'.

The texture coefficient (Tc) of the ZnS_xSe_{1-x} thin films was evaluated using the relation [37],

$$T_c(hkl) = \frac{I(hkl)/I_0(hkl)}{(1/N)(\sum_N I(hkl)/I_0(hkl))} \tag{9}$$

where Tc(hkl) is the texture coefficient of the (hkl) plane, I is the measured intensity, I_0 is the JCPDS data card intensity, and N is the number of diffraction peaks. Fig. 4 shows the variation of the Tc along the < 111 > , < 220 > and < 311 > directions with 'x'. From Fig. 4, it is seen that the texture coefficient of the ⟨111⟩ direction increases as x increases from 0.0 to 0.2. When x increases above 0.2, there is a slight decrease in Tc. The texture coefficients of < 220 > and < 311 > directions have similar trends, with smaller values compared with the < 111 > direction, confirming that the films are oriented along the < 111 > direction. The development of similar composition dependent < 111 > oriented $ZnS_{1-x}Se_x$ alloy nanowire arrays has been reported by Liang and colleagues [38]. Table 2 shows the values of Texture coefficient (Tc(hkl)) of the (hkl) plane for spray deposited of ZnS_xSe_{1-x} ($0.0 \le x \le 1.0$) thin films.

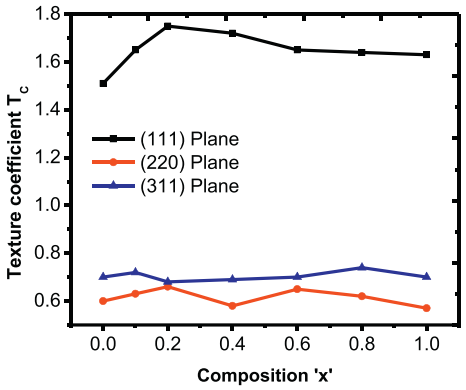

Fig. 4. Variation of texture coefficient (Tc(hkl)) of the (h k l) plane with composition '*x*' for spray deposited ZnS_xSe_{1-x} thin films.

3.3. SEM and EDS studies

Fig. 5 (a–f) shows SEM images of ZnS_xSe_{1-x} thin films with different values of 'x' at a magnification of 40,000. The measuring bar represents 2 μm. The spray deposited ZnS_xSe_{1-x} thin films are composed of uniform spherical particles, and the films become more and more compact with the increasing 'x' up to a value of 0.2. The films with x values of 0.0, 0.2 and 0.4 exhibits reasonable coverage of the surface. The surface morphology of ZnSe is different from that of ZnS. The surface morphology of the thin films gradually changes with changing 'x', as seen from Fig. 5. The change in morphology with the value of 'x' can be ascribed to the reaction mechanism. A similar morphology has been reported by Liu et al. [39] for ZnS_xSe_{1-x} thin films grown using cluster-by-cluster deposition.

Fig. 6 shows the EDS spectrum of a spray deposited $ZnS_{0.2}Se_{0.8}$ thin film. The EDS results and the atomic percentages of Zn, S and Se of the thin films are presented in Table 3 for different values of x. The EDS studies show that the ZnS_xSe_{1-x} thin films are nearly stoichiometric.

Table 2
Texture coefficient ($T_c(hkl)$) of the (*h k l*) plane for spray deposited of ZnS_xSe_{1-x} ($0.0 \le x \le 1.0$) thin films.

Composition	Texture coefficient		
	111	220	311
ZnSe	1.51	0.60	0.70
$ZnS_{0.1}Se_{0.9}$	1.65	0.63	0.72
$ZnS_{0.2}Se_{0.8}$	1.75	0.66	0.68
$ZnS_{0.4}Se_{0.6}$	1.72	0.58	0.69
$ZnS_{0.6}Se_{0.4}$	1.65	0.65	0.70
$ZnS_{0.8}Se_{0.2}$	1.64	0.62	0.74
ZnS	1.63	0.57	0.70

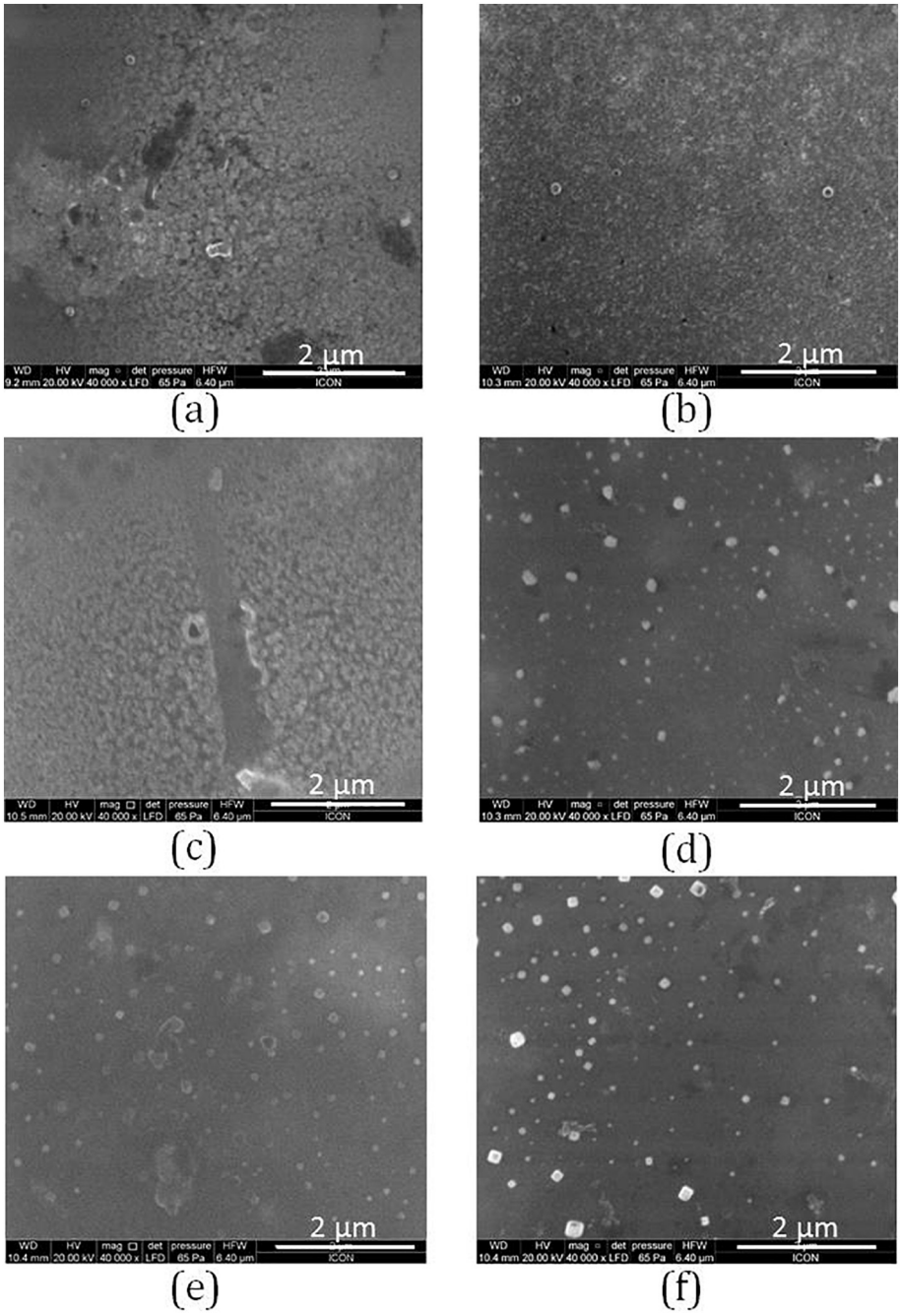

Fig. 5. SEM images of spray deposited ZnS_xSe_{1-x} thin films (a) $x = 0.0$, (b) $x = 0.2$, (c) $x = 0.4$, (d) $x = 0.6$, (e) $x = 0.8$, and (f) $x = 1.0$, respectively.

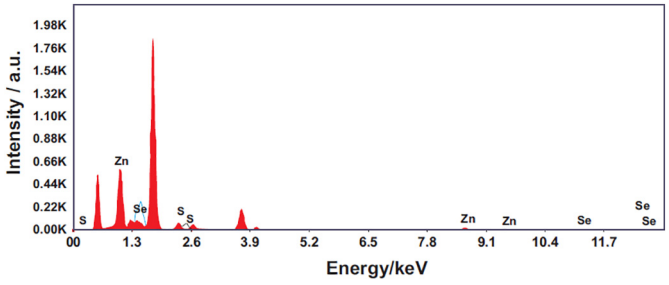

Fig. 6. EDS spectra of spray deposited $ZnS_{0.2}Se_{0.8}$ thin film.

Table 3
Elemental composition of spray deposited of ZnS_xSe_{1-x} ($0.0 \leq x \leq 1.0$) thin films.

Composition	Initial composition in spraying solution (%)			Atomic percentage in film by EDS analysis (%)		
	Zn	S	Se	Zn	S	Se
ZnSe	50.0	0.0	50.0	50.0	0.0	50.0
$ZnS_{0.2}Se_{0.8}$	50.0	10.0	40.0	50.1	09.5	40.4
$ZnS_{0.4}Se_{0.6}$	50.0	20.0	30.0	48.0	20.8	31.2
$ZnS_{0.6}Se_{0.4}$	50.0	30.0	20.0	49.7	29.2	21.1
$ZnS_{0.8}Se_{0.2}$	50.0	40.0	10.0	49.5	39.6	10.9
ZnS	50.0	50.0	0.0	50.4	49.6	0.0

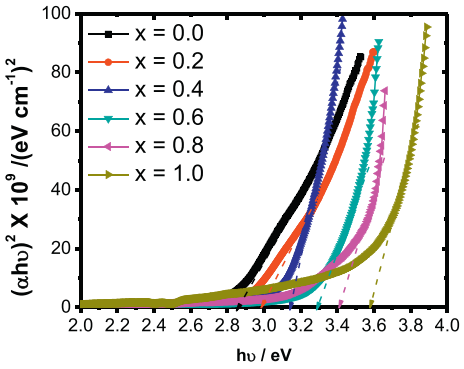

Fig. 7. Plot of $(\alpha h\upsilon)^2$ versus hυ for spray deposited ZnS_xSe_{1-x} thin films.

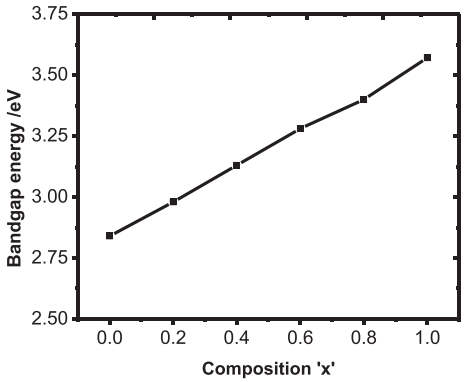

Fig. 8. Variation of optical band gap energy with composition '*x*' for spray deposited ZnS_xSe_{1-x} thin films.

3.4. Optical studies

The optical absorbance of the thin films was measured in the wavelength range 250–850 nm using a UV–Visible spectrophotometer. From the optical absorption spectra (not shown here) it was found that the films have a high coefficient of absorption ($10^4\ cm^{-1}$). The optical band gap energy (Eg) and the nature of the transition involved were determined using Tauc's relation,

$$\alpha h\upsilon = A(h\upsilon - Eg)^n \quad (10)$$

where α is the coefficient of absorption, A is a constant, hυ is the photon energy and n indicates the type of transition, (n = ½ for direct allowed transitions and n = 2 for indirect transitions). In the case of a direct band gap transition,

$$\alpha h\upsilon = A(h\upsilon - Eg)^{1/2} \quad (11)$$

Fig.7 shows plots of $(\alpha h\upsilon)^2$ versus hυ for ZnS_xSe_{1-x} thin films. The linear nature of the graph indicates a direct allowed type transition. The band gap energies were determined from the intercepts of the $(\alpha h\upsilon)^2$ versus hυ plots on the energy axis (x-axis). Table 4 shows the values of the band gap energy for the spray deposited ZnS_xSe_{1-x} thin films. A band gap value of 2.84 eV is observed for ZnSe (x = 0.0). This value of the band gap energy is slightly higher than the standard value of 2.71 eV of ZnSe [40] and is comparable with the value of 2.80 eV reported by Chadi et al. for ZnSe [41]. The optical band gap of ZnS (x = 1.0) was found to be 3.57 eV. This value is lower than the standard value of 3.67 eV [40], and is comparable with the value of 3.51 eV reported by Cao and coworkers [42] for ZnS thin films grown using a solvothermal method. The variation of Eg with 'x' is shown in Fig. 8. The values of the band gap energies match well with the values reported for zinc sulfur selenide [26]. A systematic shift in the energy band gap as a function of 'x' can be seen clearly. Fig.8 shows that the band gap increases from 2.84 eV (ZnSe) to 3.57 eV (ZnS) as the sulfur concentration in the ZnS_xSe_{1-x} increases. This band gap energy variation confirms the formation of a solid solution in ZnSSe. These results match well with those of XRD, SEM and EDS studies. Similar results have been reported by Agawane et al. [27] for chemical bath-deposited ZnSSe thin films.

Table 4
Optical and electrical properties of spray deposited of ZnS_xSe_{1-x} ($0.0 \le x \le 1.0$) thin films.

Composition	Band gap	Electrical resistivity (Ωcm)		Activation energy (eV)	
	E_g (eV)	300 K (× 10^6)	500 K (× 10^2)	L.T.	H.T.
ZnSe	2.84	2.04	1.23	0.09	0.14
$ZnS_{0.2}Se_{0.8}$	2.98	0.85	0.49	0.07	0.11
$ZnS_{0.4}Se_{0.6}$	3.13	4.90	2.69	0.11	0.15
$ZnS_{0.6}Se_{0.4}$	3.28	10.5	5.62	0.12	0.20
$ZnS_{0.8}Se_{0.2}$	3.40	24.0	12.0	0.13	0.22
ZnS	3.57	58.9	35.5	0.14	0.24

(L.T. - low temperature; H.T. - high temperature).

3.5. Electrical studies

Electrical resistivity measurements of the spray deposited ZnS_xSe_{1-x} thin films were carried out using the DC two point probe technique in the dark in the temperature range from room temperature to 500 K. The "two-bar" pattern was used to apply silver paste (thickness of silver painted bar, 1 mm; the length of bar, 1 cm; gap between two bars, 1 cm) on the thin films. Fig. 9 shows the variations of log ρ (resistivity) versus the inverse of the absolute temperature ($1/T \times 10^{-3}$) of spray deposited ZnS_xSe_{1-x} thin films. From this figure, it is clear that the resistivity decreases with increasing temperature, indicating typical semiconducting behavior. The electrical resistivities of the ZnS_xSe_{1-x} thin films are presented in Table 4. The observed room temperature electrical resistivity of ZnSe thin films is $2.04 \times 10^6\ \Omega$ cm, which is lower than the value of $45.7 \times 10^6\ \Omega$ cm reported by Sharma et al. [43] for ZnSe thin films. It was found that the electrical resistivity decreases upto x = 0.2 (0.85×10^6 Ωcm) and increases when x is increased further to 1.0 (ZnS, $58.9 \times 10^6\ \Omega$ cm). The decrease can be ascribed to an increase in the carrier concentration as a result of the replacement of Se atoms with S atoms. However, the resistivity of the ZnS_xSe_{1-x} films, increases gradually with x after reaching a minimum at x = 0.2.

Fig. 9 also shows two separate temperature zones with two different characteristic regions. The first region between room temperature and 333 K, is the low-temperature region, and the second region, between 333 and 500 K is the high-temperature region. The temperature dependence of the electrical resistivity in the low-temperature region can be attributed to an extended state conduction mechanism. In the high-

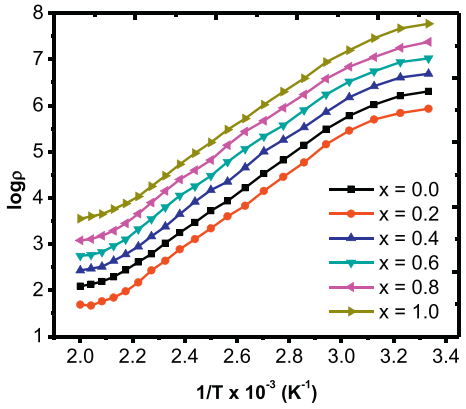

Fig. 9. Variation of logρ versus $1/T \times 10^{-3}$ for spray deposited ZnS_xSe_{1-x} thin films.

temperature region the electronic transport properties of semiconductor thin films are strongly influenced by their structural characteristics (the crystallite shape and size, inter crystal boundaries, lattice defects, etc.) and purity (nature and concentration of the impurities, adsorbed and absorbed gases, etc). So, the conduction mechanism in ZnS_xSe_{1-x} films can be explained on the basis of Seto's model [44]. The activation energies of the ZnS_xSe_{1-x} films were determined using the Arrhenius relation [45],

$$\rho = \rho_1 \exp\left(\frac{E_{a1}}{kT}\right) + \rho_2 \exp\left(\frac{E_{a2}}{kT}\right) \quad (12)$$

where ρ_1 and ρ_2 are resistivities, k is the Boltzmann constant and T is the absolute temperature. The two terms in eq. (12) arise from two different conduction mechanisms. The first term describes the high-temperature region, and the dominant mechanism is band conduction through the extended states. The second term of that equation describes the conduction process at the lower-temperature region. The activation energies of the ZnS_xSe_{1-x} thin films are presented in Table 4. Due to the contribution from free-to-bound transitions, we observed that the ZnS_xSe_{1-x} thin films have low activation energies [46].

4. Conclusions

Polycrystalline ZnS_xSe_{1-x} ($0.0 \le x \le 1.0$) thin films were successfully grown using computerized chemical spray pyrolysis on glass substrates. XRD studies revealed a cubic crystal structure with a preferential < 111 > orientation. There is a shift in the XRD peak < 111 > from 27.29° to 28.15° with an increase the sulfur content of the films, indicating the formation of solid solutions. The lattice constant decreased linearly with increasing sulfur content in the films according to Vegard's law. The crystallite size was in the range 18–28 nm. SEM studies revealed that the deposition was uniform. The EDS pattern shows that the ZnS_xSe_{1-x} thin films contain Zn, S and Se in appropriate percentages. Optical studies show that the coefficient of absorption is large and that transitions are of the direct allowed type. The band gap energy increases from 2.84 eV to 3.57 eV as the S concentration is increased. The electrical resistivity decreases as the temperature increases, indicating semiconducting behavior. The ZnS_xSe_{1-x} thin films are semiconducting in nature, with better structural, compositional, optical and electrical properties with x = 0.2 and can be used in optoelectronic devices. The tunable band gap makes these thin films suitable for solar cell applications.

References

[1] T.C.M. Santhosh, V. Kasturi, Bangeraa, Shivakumar G. K, Effect of Bi doping on the properties of CdSe thin films for optoelectronic device applications, Mater Sci Semicond Process 68 (2017) 114–117.

[2] M. Imran, Abida Saleem, Nawazish A. Khan, A.A. Khurram, Nasir Mehmood, Amorphous to crystalline phase transformation and band gap refinement in ZnSe thin films, Thin Solid Films 648 (2018) 31–38.

[3] A. Karimi, B. Sohrabi, M.R. Vaezi, Highly transparent, flexible and hydrophilic ZnS thin films prepared by a facile and environmentally friendly chemical bath deposition method, Thin Solid Films 651 (2018) 97–110.

[4] M.S. Al-Kotb Jumana, Z. Al-Waheidi, M.F. Kotkata, Investigation on microstructural and optical properties of nano-crystalline CdSe thin films, Thin Solid Films 631 (2017) 219–226.

[5] Yibing Xie, Photoelectrochemical performance of cadmium sulfide quantum dots modified titania nanotube arrays, Thin Solid Films 598 (2016) 115–125.

[6] V. Kumar, J.K. Singh, G.M. Prasad, Elastic properties of elemental, binary and ternary semiconductor materials, Ind J Pure Appl Phy 53 (2015) 429–435.

[7] Brynmor E. Jones, Peter J. Schlosser, Joel De Jesus, Thor A. Garcia, Maria C. Tamargo, Jennifer E. Hastie, Processing and characterisation of II–VI ZnCdMgSe thin film gain structures, Thin Solid Films 590 (2015) 84–89.

[8] Gary Hodes, A thin-film polycrystalline photoelectrochemical cell with 8% solar conversion efficiency, Nature 285 (1980) 29–30.

[9] M.S. Subhash Chander, Dhaka, Optical and structural constants of CdS thin films grown by electron beam vacuum evaporation for solar cells, Thin Solid Films 638 (2017) 179–188.

[10] Amruta Mutalikdesai, Sheela K. Ramasesha, Solution process for fabrication of thin film CdS/CdTe photovoltaic cell for building integration, Thin Solid Films 632 (2017) 73–78.

[11] E.A. Sanchez-Ramirez, M.A. Hernandez-Perez, J.R. Aguilar-Hernandez, G. Contreras-Puente, Bath atomic composition and deposition time influence on the properties of nanostructured $CdS_{0.5}Se_{0.5}$ thin films synthesized by CBD, Mater Chem Phy 165 (2015) 119–124.

[12] F.C. Jain, ZnSe-ZnS_xSe_{1-x} and ZnSe-$ZnS_xSe_{1-x}Mn_xSe$ metal insulator-semiconductor heterostructure lasers, J Crystal Growth 86 (1988) 929–934.

[13] P. Kannappan, K. Asoka, J.B.M. Krishna, R. Dhanasekaran, Effect of SHI irradiation on structural, surface morphological and optical studies of CVT grown ZnSSe single crystals, J Alloys Comp 580 (2013) 284–289.

[14] Y.P. Venkata Subbaiah, K.T. Ramakrishna Reddy, Structural behaviour of ZnS_xSe_{1-x} films deposited by close-spaced evaporation, Mater Chem Phy 92 (2005) 448–452.

[15] Mustafa Öztaş, Yalova Üniver Metin Bedir, Effect of nitrogen ion implantation on the sprayed ZnSe thin films, Mater. Lett. 61 (2007) 343–346.

[16] G.M. Lohar, S.K. Shinde, V.J. Fulari, Structural, morphological, optical and photoluminescent properties of spray-deposited ZnSe thin film, J. Semicond. 35 (2014) 113001–113005.

[17] S. Fridjine, S. Touihri, K. Boubaker, M. Amlouk, Some physical investigations on $ZnS_{1-x}Se_x$ films obtained by selenization of ZnS sprayed films using the Boubaker polynomials expansion scheme, J Cry Growth 312 (2010) 202–208.

[18] A.A. Yadav, E.U. Masumdar, Optical and electrical transport properties of spray deposited $CdS_{1-x}Se_x$ thin films, J Alloys Comp 505 (2010) 787–792.

[19] A. Ganguly, S. Chaudhuri, A.K. Pal, Synthesis of ZnS_xSe_{1-x} ($0 < x < 1$) nanocrystalline thin films by high-pressure sputtering, J. Phys. D. Appl. Phys. 34 (2001) 506–513.

[20] D. Seghier, J.T. Gudmundsson, H.P. Gislason, Direct observation of hydrogen passivation of nitrogen-related energy levels in ZnSe and ZnS_xSe_{1-x} grown by MBE, J Crystal Growth 214 (215) (2000) 478–481.

[21] Sunghoon Park, Hyunsu Kim, Changhyun Jin, Chongmu Lee, Synthesis, structure, and photoluminescence properties of ZnSSe alloy nanorods, Curr Appl Phy 12 (2012) 499–503.

[22] Nyen-Ts Chen, Meiso Yokoyama, Herng-Yih Ueng, Atomic layer epitaxy growth of ZnS_xSe_{1-x} epitaxial layers lattice-matched to Si substrates, J Crystal Growth 216 (2000) 152–158.

[23] Wallace B. Leigh, Bruce W. Wessels, Vapor growth and properties of thin film ZnS_xSe_{1-x}, Thin Solid Films 97 (1982) 221–229.

[24] Lin-Jer Chen, Jia-Heng Dai, Growth, morphological and optical characteristics of ZnSSe nanorods, Opt. Mater. 64 (2017) 356–360.

[25] T.P. Vipin Kumar, Sharma, Structural and optical properties of sintered ZnS_xSe_{1-x} films, Opt. Mater. 10 (1998) 253–256.

[26] S. Armstrong, P.K. Datta, R.W. Miles, Properties of zinc sulfur selenide deposited using a close-spaced sublimation method, Thin Solid Films 403-404 (2002) 126–129.

[27] G.L. Agawane, Seung Wook Shin, S.A. Vanalakar, A.V. Moholkar, K.V. Gurav, M.P. Suryawanshi, Jeong Yong Lee, Jae Ho Yun, Jin Hyeok Kim, Non-toxic novel route synthesis and characterization of nanocrystalline ZnS_xSe_{1-x} thin films with tunable band gap characteristics, Mater Res Bull 55 (2014) 106–113.

[28] K.T. Ramakrishna Reddy, Y.V. Subbaiah, T.B.S. Reddy, D. Johnston, I. Forbes, R.W. Miles, Pyrolytic spray deposition of ZnS_xSe_{1-x} layers for photovoltaic applications, Thin Solid Films 431-432 (2003) 340–343.

[29] S. Fridjine, K. Boubaker, M. Amlouk, Some electron probe X-ray microanalysis (EPMA)- and (BPES)-related physical investigations on ZnSSe thin-films growth composition-related kinetics, Canadian J Phy 87 (2009) 653–657.

[30] S. Fridjine, K.B. Ben Mahmoud, M. Amlouk, M. Bouhafs, A study of sulfur/selenium substitution effects on physical and mechanical properties of vacuum-grown $ZnS_{1-x}Se_x$ compounds using Boubaker polynomials expansion scheme (BPES), J Alloys Comp 479 (2009) 457–461.

[31] A.A. Yadav, M.A. Barote, E.U. Masumdar, Studies on cadmium selenide (CdSe) thin films deposited by spray pyrolysis, Mater Chem Phy 121 (2010) 53–57.

[32] A.A. Yadav, E.U. Masumdar, A.V. Moholkar, M. Neumann-Spallart, C.H. Bhosale, Electrical, structural and optical properties of SnO_2:F thin films: Effect of the substrate temperature, J Alloys Comp 488 (2009) 350–355.

[33] A.A. Yadav, M.A. Barote, P.M. Dongre, E.U. Masumdar, Studies on growth and characterization of $CdS_{1-x}Se_x$ ($0.0 \le x \le 1.0$) alloy thin films by spray pyrolysis, J Alloys Comp 493 (2010) 179–185.

[34] A.M. AL-Diabat, Naser M Ahmed, M.R. Hashim, Khaled M. Chahrour, M. Bououdina, Effect of deposition temperature on structural and optical properties of chemically sprayed ZnS thin films, Proc Chem 19 (2016) 485–491.

[35] Kanta Yadav, Neena Jaggi, Effect of Ag doping on structural and optical properties of ZnSe nanophosphors, Mater Sci Semicon Proc. 30 (2015) 376–380.

[36] B.D. Cullity, S.R. Stock, Elements of X-Ray Diffraction, 3rd Ed., Prentice-Hall Inc. (2001) 167–171.

[37] A.A. Yadav, M.A. Barote, T.V. Chavan, E.U. Masumdar, Influence of indium doping on the properties of spray deposited $CdS_{0.2}Se_{0.8}$ thin films, J Alloys Comp 509 (2011) 916–921.

[38] Y. Liang, H.Y. Xu, S.K. Hark, E.U. Masumdar, Epitaxial growth and composition-dependent optical properties of vertically aligned $ZnS_{1-x}Se_x$ alloy nanowire arrays, Crystal Growth Design 10 (2010) 4206–4210.

[39] Jun Liu, Ai Xiang Wei, Mi Xue Zhuang, Yu Zhao, Investigation of the ZnS_xSe_{1-x} thin films prepared by chemical bath deposition, J Mater Sci: Mater Electron 24 (2013) 1348–1353.

[40] Gertrude F. Neumark, Yinyan Gong, Igor L. Kuskovsky, Doping aspects of Zn-based wide band gap semiconductors, in: Safa Kasap, Peter Capper (Eds.), Handbook of Electronic and Photonic Materials, 32 Springer Publications, 2006, pp. 843–851.

[41] D.J. Chadi, Doping in ZnSe, ZnTe, MgSe, and MgTe wide-band-gap semiconductors, Phys Rev. Lett 72 (1994) 534–537.

[42] Jian Cao, Jinghai Yang, Yongjun Zhang, Lili Yang, Yaxin Wang, Maobin Wei, Yang Liu, Ming Gao, Xiaoyan Liu, Zhi Xie, Optimized doping concentration of manganese in zinc sulfide nanoparticles for yellow-orange light emission, J Alloys Comp 486 (2009) 890–894.
[43] Jeewan Sharma, Deep Shikha, S.K. Tripathi, Optical and electrical properties of ZnSe thin films: effect of vacuum annealing, Romanian Reports Phy 66 (2014) 1002–1011.
[44] J. Sharma, S.K. Tripathi, Effect of deposition pressure on structural, optical and electrical properties of zinc selenide thin films, Physica B 406 (2011) 1757–1762.
[45] A.S. Hassanien, Alaa A. Akl, Electrical transport properties and Mott's parameters of chalcogenide cadmium sulphoselenide bulk glasses, J Non-Crystalline Solids 432 (2016) 471–479.
[46] M. Popa, I. Tiginyanu, V. Ursaki, Mott type electrical conductivity in ZnS_xSe_{1-x} thin films, Romanian J Phy 62 (602) (2017) 1–14.